

Published in final edited form as:

Bioorg Med Chem. 2011 January 15; 19(2): 852–860. doi:10.1016/j.bmc.2010.12.017.

Syntheses, Structures and Antibiotic Activities of LpxC Inhibitors Based on the Diacetylene Scaffold

Xiaofei Liang^{a,b}, Chul-Jin Lee^{c,d}, Xin Chen^b, Hak Suk Chung^c, Daina Zeng^c, Christian R. H. Raetz^c, Yaoxian Li^a, Pei Zhou^{b,c,d,*}, and Eric J. Toone^{b,c,d,*}

^a Department of Chemistry, Jilin University, Changchun, Jilin 130021, P.R. China

^b Department of Chemistry, Duke University, Durham, NC 27708, USA

^c Department of Biochemistry, Duke University Medical Center, Durham, NC 27710, USA

^d Structural Biology & Biophysics Program, Duke University, Durham, NC 27710, USA

Abstract

Compounds inhibiting LpxC in the lipid A biosynthetic pathway are promising leads for novel antibiotics against multidrug-resistant Gram-negative pathogens. We report the syntheses and structural and biochemical characterizations of LpxC inhibitors based on a diphenyl-diacetylene (1,4-diphenyl-1,3-butadiyne) threonylhydroxamate scaffold. These studies provide a molecular interpretation for the differential antibiotic activities of compounds with a substituted distal phenyl ring as well as the absolute stereochemical requirement at the C2, but not C3, position of the threonyl group.

Keywords

LpxC; inhibitor; antibiotic; diphenyl-diacetylene; 1,4-diphenyl-1,3-butadiyne; hydroxamate

1. Introduction

Lipid A, the hydrophobic membrane anchor of lipopolysaccharide, is the major lipid component of the outer leaflet of the outer membrane of Gram-negative bacteria.^{1, 2} Because lipid A is essential for the viability of the vast majority of Gram-negative bacteria, the zinc-dependent UDP-3-*O*-(acyl)-*N*-acetylglucosamine deacetylase (LpxC), which catalyzes the first irreversible step in lipid A biosynthesis, has become an attractive target for the development of novel therapeutics for treatment of multidrug-resistant Gram-negative infections.³ Indeed, a large number of compounds with vastly different chemical scaffolds targeting LpxC have been reported in both the scientific^{4, 5} and patent^{6–14} literature.

*Corresponding authors. Tel.: (919) 681-3484. toone@chem.duke.edu (E. J. Toone); Tel.: (919) 668-6409. peizhou@biochem.duke.edu (P. Zhou).

Supplementary data

Supplementary data include synthetic procedures for intermediates **6** and **11**, *D*-threonine methyl ester hydrochloride and *allo-D*-threonine methyl ester hydrochloride, X-ray crystallographic statistics, and PCR primers.

Publisher's Disclaimer: This is a PDF file of an unedited manuscript that has been accepted for publication. As a service to our customers we are providing this early version of the manuscript. The manuscript will undergo copyediting, typesetting, and review of the resulting proof before it is published in its final citable form. Please note that during the production process errors may be discovered which could affect the content, and all legal disclaimers that apply to the journal pertain.

Among the well-characterized compounds, **CHIR-090** based on the diphenyl-acetylene scaffold (Table 1) is the most potent LpxC inhibitor reported to date, and it is the first reported compound that effectively kills both *Escherichia coli* (*E. coli*) and *Pseudomonas aeruginosa* (*P. aeruginosa*) in bacterial disk diffusion assays.¹⁵ Because *P. aeruginosa* is a predominant cause of morbidity and mortality in cystic fibrosis patients and can cause a variety of infections, particularly in immunosuppressed individuals, the discovery of potent antibiotic activity of **CHIR-090** against *P. aeruginosa* has generated significant interest in further developing LpxC inhibitors as novel antibiotics for treatment of multidrug-resistant *Pseudomonas* and other Gram-negative infections. However, **CHIR-090** is about 600-fold less effective against LpxC orthologs from the *Rhizobium* family than against *E. coli* LpxC, which raises concerns surrounding rapid evolution of antibiotic resistance for **CHIR-090** sensitive strains through point mutations.¹⁶ Our recent structural and biochemical studies of the LpxC/**CHIR-090** complex suggest that van der Waals (vdW) clashes between the phenyl ring distal to the hydroxamate group of **CHIR-090** and LpxC residues at the substrate-binding passage result in a large decrease in **CHIR-090** activity against LpxC orthologs of the *Rhizobium* family.¹⁷ This study has motivated us to investigate the antibiotic profiles of LpxC inhibitors based on a chemical scaffold of reduced radius, such as the diacetylene (1,3-butadiyne) backbone. Recently, we showed that the 1,4-diphenyl-1,3-butadiyne (referred to as diphenyl-diacetylene below) derived **LPC-009** (Table 1), which is one of the many structures listed in the international patent WO 2004/062601 A2,⁶ effectively diminishes the resistance to **CHIR-090** by 20-fold for LpxC enzymes from the *Rhizobium* family of bacteria and enhances the antibiotic activity against *E. coli* and *P. aeruginosa* by 2–4 fold over **CHIR-090**.¹⁸ Although diacetylene-based LpxC inhibitors have appeared in a number of international patents,^{6, 8} there is a lack of synthetic details for these compounds. The potency, spectrum of inhibition, and structure-activity relationship of these compounds have not been systematically characterized. In addition, the diphenyl-diacetylene compound **LPC-009** has limited solubility in aqueous solution. In order to improve the solubility and probe the stereochemical requirement of the threonyl group of **LPC-009**, we have carefully selected from published patents^{6, 8} a set of **LPC-009** amino derivatives and designed additional compounds based on structural insights from the LpxC/**LPC-009** complexes.¹⁸ These compounds were synthesized using optimized procedures. Through detailed biochemical assays and structural characterizations of these LpxC-inhibitor interactions, we reveal the molecular basis underlying the observed structure-activity relationship of **LPC-009** amino derivatives as well as the stereochemical requirement of the threonyl head group.

2. Results

2.1. Synthesis

Synthesis of **LPC-011** began with acylation of *L*-threonine methyl ester using sodium 4-ethynylbenzoate **1** (Scheme 1). Under modified Glaser coupling conditions,^{19, 20} the resulting 4-ethynylbenzamide **2** was coupled with 4-ethynylbenzenamine to afford diacetylene methyl ester **3a**. Finally, the methyl ester was converted to the corresponding hydroxamic acid (**LPC-011**) by treatment with hydroxylamine under basic conditions. Regioisomers **LPC-012** and **LPC-013** were synthesized through the same procedure. 2-Ethynylbenzenamine was very sluggish to proceed the Glaser coupling with 4-ethynylbenzamide **2**; the isolated yield was only 26% even after 80 h reaction at room temperature. Elevated temperature did not improve the yield.

In order to study the effect of threonyl chirality on **LPC-011** inhibitory activity, three diastereoisomers of **LPC-011** were synthesized (Scheme 2). For convergence of the synthesis, 4-[(4'-aminophenyl)buta-1,3-diyne-1-yl]benzoic acid **6**⁶ was prepared in 4-steps: Sonogashira coupling²¹ of methyl 4-iodobenzoate with (trimethylsilyl)-acetylene, followed

by treatment with potassium carbonate to afford methyl 4-ethynylbenzoate **4**. Employing a similar procedure for **3a-c**, **4** was coupled with 4-ethynylbenzenamine to give diacetylene methyl ester **5**. Upon hydrolysis with NaOH, diacetylene acid **6** was obtained from **5** in 90% yield.

For the preparation of *allo*-*L*-threonine methyl ester **11** with the *S* absolute configuration at C3 position, *L*-threonine methyl ester (**8**) was acylated with benzoyl chloride to generate *N*-benzoyl amino ester **9**. **9** was treated with thionyl chloride¹⁷ on ice to give oxazoline **10**, establishing the *S* absolute configuration at C5.^{22, 23} Acid hydrolysis of **10** in boiling 6 N HCl aqueous solution resulted in *allo*-*L*-threonine. This compound was converted to the corresponding methyl ester hydrochloride **11** (Scheme 2). Under standard amide coupling conditions (EDC/HOBT/DIEA), **11** was reacted with diacetylene acid **6** to give diacetylene amide **7** in 90% yield. Finally, the methyl ester was converted to the corresponding hydroxamic acid (**LPC-053**) by treatment with hydroxylamine under basic conditions.

Diastereoisomer **LPC-054**, which incorporates the *R* absolute configuration at both C2 and C3 began from *D*-threonine. *D*-threonine was refluxed with thionyl chloride in MeOH to produce the corresponding methyl ester hydrochloride, and then coupled with diacetylene acid **6**, resulting in diacetylene amide methyl ester (92% yield). Treatment with hydroxylamine under basic conditions converted the methyl ester to the corresponding hydroxamic acid **LPC-054** (93% yield; Scheme 2). By employing identical procedures, enantiomer **LPC-055** with 2*R* and 3*S* configurations was obtained starting from *allo*-*D*-threonine (Scheme 2). The overall yield (~48%) for the last two steps was slightly lower than for **LPC-054**. Neither racemization nor epimerization was observed by LC-MS or NMR during the synthesis of **LPC-011-013** and **053-055** when using 25% sodium methoxide in methanol solution as the base for converting the methyl esters into the corresponding hydroxamic acids.

2.2. Structure-activity relationship

The antibiotic activities of **LPC-011-013** and **053-055** were evaluated by measuring the minimum inhibitory concentrations (MICs) against wild-type *E. coli* (W3110), *P. aeruginosa* (PAO1), and modified *E. coli* strains with the native *lpxC* gene replaced by that of *R. leguminosarum* (W3110RL) or *P. aeruginosa* (W3110PA) (Table 1).

Amino substitution of the distal phenyl ring—In general, addition of an amino group to the distal phenyl ring of **LPC-009** enhanced aqueous solubility. However, these substitutions have very different effects on antibiotic activities. The most effective compound, **LPC-011** with an amino substitution at the *para*-position of the distal phenyl ring, shows enhancement in antibiotic activity over **CHIR-090** against all of the tested bacterial strains: compared to **CHIR-090**, **LPC-011** is roughly 7-fold more potent against wild type *E. coli* W3110, 32-fold more potent against *E. coli* W3110RL, and ~3-fold more potent against *E. coli* W3110PA and *P. aeruginosa* PAO1. These results are consistent with the notion that LpxC inhibitors with the narrow diacetylene scaffold effectively overcome the resistance mechanism observed for *R. leguminosarum* LpxC,^{17, 18} and have a superior antibiotic profile compared to **CHIR-090**. Compound **LPC-011** also displays enhanced antibiotic activity (~1.5-fold) toward wild-type *E. coli* and *P. aeruginosa* compared to the parent compound **LPC-009**. In contrast, amino substitution at the *meta*-position (**LPC-012**) has little or slightly negative effect, and amino substitution at the *ortho*-position (**LPC-013**) results in a significant decrease in antibiotic activity (> 10-fold).

To probe the molecular basis for the distinct antibiotic profiles for compounds with amino substitutions at different positions (*ortho*, *meta* and *para*), we determined the crystal structures of *E. coli* LpxC in complex with the *para*-amino substituted compound **LPC-011**

and *meta*-amino substituted compound **LPC-012** (crystallographic statistics shown in Table S1 in Supplementary data). The overall structure of *E. coli* LpxC in these inhibitor-bound complexes is essentially identical to that in the *E. coli* LpxC/**LPC-009** complex.¹⁸ The threonyl-hydroxamate head group occupies the LpxC active site, the proximal phenyl group locates at the entrance of the hydrophobic substrate-binding passage, the diacetylene group penetrates through the passage, and the distal phenyl ring interacts with a cluster of hydrophobic residues, including I198, M195, F212 and V217 in *E. coli* LpxC (Fig. 1A,B). Additional electron density, which was interpreted as a buffer sulfate anion, was observed in the active site, mediating hydrogen bonds with the inhibitor threonyl group and K239 in *E. coli* LpxC.

Of all three possible positions of the distal phenyl ring, substitution at the *para*-position is best tolerated, as this position remains solvent exposed and does not generate vdW clashes with nearby residues. In addition, *para*-amino substitution of the distal phenyl group, due to its proximity to the F212 of *E. coli* LpxC, likely enhances the edge-to-face π - π interaction between the distal phenyl ring of **LPC-011** and F212 of *E. coli* LpxC, modestly increasing the activity of the *para*-amino compound **LPC-011** relative to **LPC-009** for *E. coli* (Fig. 1A). To obtain more quantitative measurements of the inhibitory effect of **LPC-011**, we performed detailed enzyme kinetic studies. Analogous to **LPC-009** but unlike the slow tight-binding inhibitor **CHIR-090**,^{15, 16, 18} we observed a similar fractional inhibition of product accumulation with or without **LPC-011** pre-incubation (1–3 h) with enzyme, suggesting that **LPC-011** does not inhibit *E. coli* LpxC in a time-dependent fashion. A K_i^{app} value of 0.20 ± 0.02 nM and a corresponding K_I value of 0.067 ± 0.007 nM were calculated for **LPC-011** based on the assumption of competitive inhibition and a measured K_M value of 2.5 ± 0.2 μ M (Fig. 1C, see *Experimental Section* for details). A 2.7-fold reduction of K_i^{app} and K_I values of **LPC-011** in comparison with **LPC-009** ($K_i^{\text{app}}=0.55 \pm 0.09$ nM and $K_I = 0.18 \pm 0.03$ nM) further supports the favorable energetic interaction between the *para*-amino substituted distal phenyl ring with F212 of *E. coli* LpxC.

Amino substitution at the *meta*-position generated different results for distinct LpxC orthologs. In the *E. coli* LpxC/**LPC-012** complex, the *meta*-amino forms a hydrogen bond with the carbonyl oxygen of the side group of Q202 (Fig. 1B), but this hydrogen bond apparently does not contribute significantly to the overall binding energy, as the activity of the *meta*-amino substituted compound is comparable to the less soluble, unsubstituted compound **LPC-009**.

In contrast to *para*- or *meta*-substitutions, an amino group at the *ortho*-position is clearly detrimental: structural modeling suggests that regardless of the orientation of the distal phenyl ring, amino substitution at the *ortho*-position generates vdW clashes with Q202 and F212 of *E. coli* LpxC and the corresponding residues in other LpxC orthologs (Fig. 1D,E). Consequently, the *ortho*-amino substituted compound **LPC-013** is substantially less effective than the parent compound **LPC-009** for all of the bacterial strains tested (>10 fold).

Stereochemistry of the threonyl group—We also investigated the stereochemical requirement for the threonine head group in **LPC-011** on its antibiotic activity using three diastereoisomers of **LPC-011**. The MIC results show that the *S*-configuration at C2 position of the threonine moiety in **LPC-011** is absolutely required for effective antibiotic activity. When the absolute configuration in C2 position is inverted from *S* to *R*, the resulting (2*R*, 3*R*)-diastereomer **LPC-054** and (2*R*,3*S*)-enantiomer **LPC-055** exhibited significantly decreased activity compared to **LPC-011** (over 100-fold for *E. coli*). On the other hand, the absolute configuration at C3 position is less critical than the stereochemistry at the C2 position. For example, the (2*S*,3*S*)-diastereomer **LPC-053** showed only a slight decrease

(1.6- to 3.2-fold) in antibiotic activity compared to the (2*S*,3*R*)-diastereomer **LPC-011** against all of tested bacterial strains.

The nearly identical activity for the C3 diastereomeric compound **LPC-053** is surprising, as the methyl group of **LPC-011** forms a critical vdW interaction with the highly conserved F192 in *E. coli* LpxC and the hydroxyl group of **LPC-011** participates in hydrogen bonds with K239 and H265. To seek a molecular understanding of the binding mode of the C3-*S* diastereomeric compound **LPC-053**, we determined its complex structure with *E. coli* LpxC (Fig. 2A, crystallographic statistics shown in Table S1 in Supplementary data). The structure reveals intact vdW interactions between the methyl group of **LPC-053** and the F192, highlighting their significant energetic contribution to the binding affinity. In contrast, the hydroxyl group in **LPC-053** points away from the active site and is unable to form *direct* hydrogen bonds with K239 and H265 as the C3-*R* compound **LPC-011**. Interestingly, the loss of hydrogen bonds in **LPC-011** (2*S*, 3*R*) is compensated by the formation of a water-mediated hydrogen bond between the hydroxyl group in **LPC-053** (2*S*, 3*S*) and the carbonyl oxygen of F192 (Fig. 2A). Similar to the **LPC-011** and **LPC-012** complex, additional density was observed in the active site, which was interpreted as a sulfate anion from the buffer. The energetic contribution of the sulfate group to **LPC-053** binding to LpxC is unclear, but the sulfate group is well-positioned to form hydrogen bonds with the hydroxyl group of **LPC-053** and K239 of *E. coli* LpxC. Thus the change of the stereochemistry at the C3 position only has a limited effect (< 3.5-fold) on the overall antibiotic activity. In contrast, the stereochemistry at the C2 position is critical: with the same overall binding mode, alteration of the C2 stereochemistry from *S* to *R*—regardless of the rotameric state of the threonyl side-chain—generates vdW clashes with residues (such as C63 in *E. coli* LpxC) in the Insert I loop (Fig. 2B,C), resulting in significantly reduced antibiotic activities for compounds **LPC-054** and **LPC-055**.

3. Discussion and conclusion

Most of the LpxC inhibitors reported in the literature are limited by their spectrum of antibiotic activities. The structural prediction and experimental validation of broad-spectrum antibiotic activities of LpxC inhibitors based on the diacetylene moiety—a chemical scaffold initially reported in the international patent WO 2004/062601 A2—are an important step forward in the search for better antibiotics targeting LpxC. To improve the solubility of **LPC-009** in aqueous solution and to probe the stereochemical requirement of the threonyl group, we investigated the structures and antibiotic profiles of **LPC-009** derivatives. Although all three amino substituents of the distal phenyl ring (**LPC-011-013**) have improved solubility in aqueous solution, they have very different antibiotic profiles. The *para*-amino substituent **LPC-011** slightly enhances the antibiotic activity of the parent compound **LPC-009**, and has a 2.7-fold lower K_I value than that of **LPC-009** against *E. coli* LpxC. The *para*-position is largely exposed to solvent, suggesting that even more extensive functionality can be tolerated. Therefore, it might be possible to replace the *para*-amino group with a fluorophore or an azide group without significantly affecting its antibiotic activity. This may allow the development of fluorescence-based inhibitor binding assays or new tools based on click chemistry via Cu(I)-catalyzed azide-alkyne cycloaddition²⁴ for affinity purification and identification of human metalloproteins that tightly associate with LpxC inhibitors in cells—a particular concern for the unintended off-target activity of hydroxamate-containing compounds.

Stereochemistry is an important factor of inhibitor design. We show that the *R*-stereoisomer at the C2 position of the threonyl group is detrimental to the antibiotic profiles of **LPC-011** derivatives. In contrast, the chirality at the C3 position of the threonyl group is less stringent, and compounds with either *S*- or *R*-configurations at the C3 position show similar antibiotic

activities for tested bacterial strains. Our structural investigation reveals an invariant threonyl methyl-F192 interaction regardless of the stereochemistry at the C3 position. However, the loss of favorable hydrogen bonds between the hydroxyl group in the 3*R* configuration of **LPC-011** and K239 and H265 of *E. coli* LpxC is compensated by a water mediated hydrogen bond with the carbonyl group of F192 of *E. coli* LpxC involving the same hydroxyl group in the 3*S* configuration of **LPC-053** pointing away from the active site toward the solvent. Previous structural studies of the LpxC/UDP complex have revealed a UDP-binding pocket that is located adjacent to the active site occupied by the threonyl head group of **CHIR-090**.^{17, 25, 26} Recently, uridine-based compounds have been shown to inhibit LpxC *in vitro*, presumably by competing for the same UDP-binding pocket with the LpxC substrate UDP-3-*O*-(acyl)-*N*-acetylglucosamine.²⁷ Because the hydroxyl group in the 3*S* compound **LPC-053** is solvent exposed, it may be a convenient functional group for further derivatization to extend the current compound binding interface to the adjacent UDP-binding pocket and generate more potent inhibitors based on the well-known ligand additivity effect.²⁸

4. Experimental section

LC/MS analysis was conducted on an Agilent 1200 HPLC with a quadrupole mass analyzer. LC chromatography used an Agilent XDB-C18 column (4.6×50 mm, 1.8 μm) with a water/acetonitrile (each with 0.2% (v/v) formic acid) gradient at a flow rate of 0.5 mL/min. HRMS analyses were performed at the Duke MS Center. Proton (¹H) and carbon (¹³C) NMR spectra were recorded at 300 and 75 MHz, respectively, on a Varian spectrometer. Column chromatography was conducted using either silica gel (Silicycle 40–64 μm) or prepacked RediSep columns (Teledyne Isco Inc., Lincoln, NE) on an Isco CombiFlash Rf instrument. All moisture-sensitive reactions were carried out using dry solvents and under a slight pressure of ultra-pure argon. Glassware was dried in an oven at 140 °C for at least 12 h prior to use, and then assembled quickly while hot, sealed with rubber septa, and allowed to cool under a stream of argon. Reactions were stirred magnetically using Teflon-coated magnetic stirring bars. Commercially available disposable syringes were used for transferring reagents and solvents.

Methyl (2*S*,3*R*)-2-[(4'-ethynylphenyl)formamido]-3-hydroxybutanoate (**2**)

To a stirred mixture of sodium 4-ethynylbenzoate **1** (2.52 g, 15 mmol) and *L*-threonine methyl ester hydrochloride (3.05 g, 18 mmol, 1.2 equiv) in anhydrous DMF (100 mL) was added *N*-ethyl-*N'*-(3-dimethylaminopropyl) carbodiimide hydrochloride (EDC.HCl) (3.45 g, 18 mmol, 1.2 equiv) and 1-hydroxybenzotriazole hydrate (HOBt) (2.45 g, 18 mmol, 1.2 equiv) at room temperature. The mixture was cooled in an ice-bath, and diisopropylethylamine (DIEA) (10.45 mL, 60 mmol, 4.0 equiv) was added. The whole reaction mixture was stirred under argon at 0 °C for 1 h, then allowed to warm to ambient temperature, and the stirring was continued for additional 20 h. The resulting yellow solution was evaporated to dryness under reduced pressure, and the resulting residue was treated with water (100 mL) and extracted with EtOAc (3×100 mL). The combined extracts were washed with 1 N HCl (2×70 mL) and brine (100 mL), and dried (anhydrous Na₂SO₄). Evaporation of the solvent afforded the crude product (3.5 g), which was crystallized from EtOAc/hexane to give **2** (1.9 g, 48% yield) as light yellow crystal. ¹H NMR (300 MHz, CDCl₃): δ 1.28 (d, *J*=6.3 Hz, 3H), 3.21 (s, 2H), 3.79 (s, 3H), 4.41–4.49 (m, 1H), 4.80 (dd, *J*=2.4, 2.4 Hz, 1H), 6.94 (d, *J*=9.0 Hz, 1H), 7.55 (d, *J*=8.4 Hz, 2H), 7.79 (d, *J*=8.7 Hz, 2H); ¹³C NMR (75 MHz, CDCl₃): δ 20.34, 52.95, 57.81, 68.42, 79.94, 82.89, 126.06, 127.39, 132.55, 133.86, 167.28, 171.74; MS (ESI, positive): *m/z* 284 [M+Na]⁺.

General procedure for Glaser coupling of 4-ethynylbenzamide **2** with ethynylbenzenamine

Copper (II) acetate (0.36 g, 2 mmol, 2.0 equiv) was added at room temperature to a stirred solution of **2** (0.26 g, 1 mmol) and substituted acetylene (5 mmol, 5 equiv) dissolved in anhydrous pyridine (4 mL) and MeOH (4 mL), and the reaction mixture was stirred at room temperature for 18 h (80 h for 3-ethynylbenzenamine and 2-ethynylbenzenamine). The resulting blue solution was concentrated to dryness with a rotavapor, and the residue was treated with water (50 mL) and extracted with EtOAc (3×50 mL). The combined organic extracts were washed with water (50 mL) and brine (50 mL), and dried (anhydrous Na₂SO₄). The crude product was purified by the CombiFlash system (eluting with 50–75% EtOAc in hexane) to afford diacetylene methyl ester **3a-c** as yellow solid.

Methyl (2S,3R)-2-{4'-[(4''-aminophenyl)buta-1',3'-diynyl]benzamido}-3-hydroxy-butanoate (**3a**)

67% yield; ¹H NMR (300 MHz, CDCl₃): δ 1.28 (d, *J*=6.3 Hz, 3H), 3.79 (s, 3H), 3.94 (br, s, 1H), 4.47–4.44 (m, 1H), 4.80 (dd, *J*=8.7, 2.4 Hz, 1H), 6.59 (d, *J*=8.7 Hz, 2H), 6.93 (d, *J*=8.4 Hz, 2H), 7.33 (d, *J*=8.7 Hz, 2H), 7.57 (d, *J*=8.4 Hz, 2H), 7.79 (d, *J*=8.4 Hz, 2H); ¹³C NMR (75 MHz, CDCl₃): δ 20.35, 52.96, 57.79, 68.44, 72.01, 79.89, 84.53, 110.51, 114.84, 126.32, 127.44, 132.72, 133.62, 134.43, 148.01, 167.21, 171.72; MS (ESI, positive): *m/z* 399 [M+Na]⁺.

Methyl (2S,3R)-2-{4'-[(3''-aminophenyl)buta-1',3'-diynyl]benzamido}-3-hydroxy-butanoate (**3b**)

62% yield; ¹H NMR (300 MHz, CDCl₃): δ 1.26 (d, *J*=6.3 Hz, 3H), 3.76 (s, 3H), 4.42–4.44 (m, 1H), 4.78 (dd, *J*=9.0, 2.4 Hz, 1H), 6.68 (d, *J*=8.1 Hz, 1H), 6.80 (s, 1H), 6.92 (d, *J*=7.5 Hz, 1H), 7.09 (t, *J*=15.6 Hz, 1H), 7.54 (d, *J*=8.7 Hz), 7.77 (d, *J*=8.4 Hz, 2H); ¹³C NMR (75 MHz, CDCl₃): δ 20.35, 52.94, 58.00, 68.35, 73.19, 80.33, 83.54, 116.79, 118.66, 122.28, 123.24, 125.88, 127.51, 129.64, 132.84, 133.89, 146.60, 167.34, 171.73; MS (ESI, positive): *m/z* 399 [M+Na]⁺.

Methyl (2S,3R)-2-{4'-[(2''-aminophenyl)buta-1',3'-diynyl]benzamido}-3-hydroxy-butanoate (**3c**)

26% yield; ¹H NMR (300 MHz, CDCl₃): δ 1.27 (d, *J*=6.3 Hz, 3H), 3.77 (s, 3H), 4.35 (br, 1H), 4.41–4.46 (m, 1H), 4.79 (dd, *J*=8.7, 2.4 Hz, 1H), 6.64–6.69 (m, 2H), 7.06 (d, *J*=8.7 Hz, 1H), 7.12–7.18 (m, 1H), 7.33 (dd, *J*=8.1, 1.5 Hz, 1H), 7.55 (d, *J*=8.7 Hz, 2H), 7.79 (d, *J*=8.4 Hz, 2H); ¹³C NMR (75 MHz, CDCl₃): δ 20.35, 52.95, 57.98, 68.37, 76.70, 98.95, 80.33, 81.81, 105.95, 114.70, 118.20, 125.87, 127.54, 131.16, 132.72, 133.38, 133.90, 149.98, 167.29, 171.73; MS (ESI, positive): *m/z* 399 [M+Na]⁺.

General procedure for preparing hydroxamic acids (LPC-011, 012, 013) from the corresponding methyl esters **3a-c**

To an ice-cold solution of **3** (120 mg, 0.32 mmol) dissolved in anhydrous MeOH (1.5 mL) and THF (1.5 mL) was added hydroxylamine hydrochloride (110 mg, 1.60 mmol, 5 equiv) followed by 25% sodium methoxide in methanol solution (0.53 mL, 2.20 mmol, 7 equiv). The reaction mixture was stirred under argon at 0 °C for 2 h, then allowed to warm to ambient temperature and stirring was continued overnight (16 h). The resulting yellow suspension was concentrated to dryness with a rotavapor, and the residue was treated water (50 mL). The mixture was extracted with EtOAc (3×50 mL). The combined organic layers were washed with brine (30 mL) and dried. Evaporation of the solvent afforded the crude product, which was purified by CombiFlash (eluting with MeOH in DCM 7–10%) to afford hydroxamic acid as yellow solid.

(2S,3R)-2-{4'-[(4''-aminophenyl)buta-1',3'-diynyl]benzamido}-1,3-dihydroxy-butanamide (LPC-011)

61% yield; ¹H NMR (300 MHz, CD₃OD): δ 1.23 (d, *J*=6.6 Hz, 3H), 4.21–4.17 (m, 1H), 4.43 (d, *J*=5.1 Hz, 1H), 6.62 (d, *J*=6.9 Hz, 2H), 7.24 (d, *J*=8.7 Hz, 2H), 7.58 (d, *J*=8.7 Hz, 2H), 7.87 (d, *J*=8.4 Hz, 2H); ¹³C NMR (75 MHz, CD₃OD): δ 57.90, 67.23, 70.73, 76.63, 78.97, 84.57, 108.32, 114.22, 126.06, 127.56, 132.07, 133.81, 150.22, 168.08, 168.41; HRMS: calculated for C₂₁H₁₉N₃O₄ 377.1376; found 377.1376 (M⁺).

(2S,3R)-2-{4'-[(3''-aminophenyl)buta-1',3'-diynyl]benzamido}-1,3-dihydroxy-butanamide (LPC-012)

66% yield; ¹H NMR (300 MHz, CD₃OD): δ 1.23 (d, *J*=6.3 Hz, 3H), 4.18–4.21 (m, 1H), 4.43 (d, *J*=5.1 Hz, 1H), 6.73–6.77 (m, 1H), 6.80–6.84 (m, 2H), 7.07 (m, 1H), 7.60 (d, *J*=8.4 Hz, 2H), 7.88 (d, *J*=8.4 Hz, 2H); ¹³C NMR (75 MHz, CD₃OD): δ 19.16, 57.91, 67.24, 71.82, 75.76, 79.52, 83.29, 116.72, 118.17, 121.69, 121.76, 125.47, 127.61, 129.18, 132.30, 134.22, 148.19, 168.02, 168.41; HRMS: calculated for C₂₁H₁₉N₃O₄ 377.1376; found 377.1369 (M⁺).

(2S,3R)-2-{4'-[(2''-aminophenyl)buta-1',3'-diynyl]benzamido}-1,3-dihydroxy-butanamide (LPC-013)

74% yield; ¹H NMR (300 MHz, CD₃OD): δ 1.23 (d, *J*=6.3 Hz, 3H), 4.18–4.22 (m, 1H), 4.44 (d, *J*=5.1 Hz, 1H), 6.59 (m, 1H), 6.74 (dd, *J*=8.1, 0.6 Hz, 1H), 7.09–7.15 (m, 1H), 7.26 (dd, *J*=1.2 Hz, 1H), 7.60 (d, *J*=8.4 Hz, 2H), 7.88 (d, *J*=6.9 Hz, 2H); ¹³C NMR (75 MHz, CD₃OD): δ 19.16, 57.92, 67.26, 75.86, 77.75, 80.21, 80.99, 105.01, 114.53, 117.03, 125.61, 127.38, 127.63, 130.87, 132.03, 132.19, 132.80, 134.14, 151.15, 168.03, 168.39; HRMS: calculated for C₂₁H₁₉N₃O₄ 377.1376; found 377.1374 (M⁺).

General procedure for synthesis of LPC-053, 054 and 055

To a stirred mixture of acid **6** (120 mg, 0.46 mmol) and *allo*-*L*-threonine methyl ester hydrochloride **11** (94 mg, 0.55 mmol, 1.2 equiv) in anhydrous DMF (5 mL) was added EDC.HCl (106 mg 0.55 mmol, 1.2 equiv), HOBt (75 mg, 0.55 mmol, 1.2 equiv) at room temperature. The mixture was chilled to 0 °C with an ice-bath, and DIEA (0.32 mL, 1.84 mmol, 4 equiv) was added. The reaction mixture was stirred under argon at 0 °C for 1 h, then allowed to warm to ambient temperature with the stirring continued for additional 18 h. The resulting yellow solution was condensed to dryness with a rotavapor, and the residue was treated with water (20 mL), extracted with EtOAc (3×50 mL). The combined extracts were washed with brine (40 mL), and dried. Evaporation of the solvent afforded the crude product, which was purified by CombiFlash (eluting with 1–3% MeOH in DCM) to afford methyl (2S,3S)-2-{4'-[(4''-aminophenyl)buta-1',3'-diynyl]benzamido}-3-hydroxybutanoate **7** (159 mg, 92% yield) as yellow solid. ¹H NMR (300 MHz, DMSO-*d*₆): δ 1.16 (d, *J*=6.3 Hz, 3H), 3.62 (s, 3H), 3.98–4.08 (m, 1H), 4.37 (t, *J*=14.4 Hz, 1H), 5.06 (d, *J*=6.0 Hz, 1H), 5.83 (br s, 2H), 6.53 (d, *J*=8.7 Hz, 2H), 7.24 (d, *J*=8.4 Hz, 2H), 7.63 (d, *J*=8.4 Hz, 2H), 7.87 (d, *J*=8.7 Hz, 2H), 8.64 (d, *J*=7.8 Hz, 1H); ¹³C NMR (75 MHz, DMSO-*d*₆): δ 21.06, 52.34, 60.14, 67.08, 71.78, 77.41, 80.78, 86.43, 105.83, 114.27, 124.96, 128.63, 132.64, 134.55, 134.70, 151.56, 166.39, 171.94; MS (ESI, positive): *m/z* 377 [M+H]⁺.

Following the similar procedure, methyl (2R,3R)-2-{4'-[(4''-aminophenyl)buta-1',3'-diynyl]benzamido}-3-hydroxybutanoate (**14**) and methyl (2R,3S)-2-{4'-[(4''-aminophenyl)buta-1',3'-diynyl]benzamido}-3-hydroxybutanoate (**16**) were obtained.

Methyl (2R,3R)-2-{4'-[(4''-aminophenyl)buta-1',3'-diynyl]benzamido}-3-hydroxy-butanoate (14)

¹H NMR (300 MHz, DMSO-d₆): δ 1.13 (d, *J*=6.0 Hz, 3H), 3.64 (s, 3H), 4.14–4.19 (m, 1H), 4.48 (m, 1H), 4.94 (d, *J*=7.5 Hz, 1H), 5.83 (br s, 2H), 6.53 (d, *J*=8.1 Hz, 2H), 7.24 (d, *J*=7.2 Hz, 2H), 7.65 (d, *J*=6.9 Hz, 2H), 7.90 (d, *J*=7.2 Hz, 2H), 8.37 (d, *J*=7.5 Hz, 1H); ¹³C NMR (75 MHz, DMSO-d₆): δ 20.92, 52.59, 59.76, 67.08, 71.77, 77.42, 80.77, 86.44, 105.82, 114.27, 125.00, 128.56, 132.71, 134.70, 151.56, 166.74, 171.69; MS (ESI, positive): *m/z* 377 [M+H]⁺.

Methyl (2R,3S)-2-{4'-[(4''-aminophenyl)buta-1',3'-diynyl]benzamido}-3-hydroxy-butanoate (16)

¹H NMR (300 MHz, DMSO-d₆): δ 1.15 (d, *J*=6.3 Hz, 3H), 3.63 (s, 3H), 4.00–4.06 (m, 1H), 4.36 (t, *J*=13.2 Hz, 1H), 5.06 (d, *J*=4.2 Hz, 1H), 5.83 (br s, 2H), 6.53 (d, *J*=6.9 Hz, 2H), 7.24 (d, *J*=6.9 Hz, 2H), 7.63 (d, *J*=6.6 Hz, 2H), 7.87 (d, *J*=8.1 Hz, 2H), 8.64 (d, *J*=6.9 Hz, 1H); ¹³C NMR (75 MHz, DMSO-d₆): δ 21.07, 52.33, 60.14, 67.06, 71.76, 77.40, 80.79, 86.43, 105.81, 114.26, 124.95, 128.63, 132.64, 134.54, 134.70, 151.56, 166.38, 171.94; MS (ESI, positive): *m/z* 377 [M+H]⁺.

To an ice-cold solution of **7** (100 mg, 0.26 mmol) dissolved in anhydrous MeOH (1 mL) and THF (1 mL) was added hydroxylamine hydrochloride (92 mg, 1.33 mmol, 5 equiv) followed by 25% sodium methoxide in methanol solution (0.47 mL, 2.0 mmol, 7.5 equiv). The reaction mixture was stirred under argon at 0 °C for 2 h, then allowed to warm to ambient temperature with the stirring continued overnight (14 h). The resulting yellow suspension was condensed to dryness with a rotavapor, and the residue was treated water (20 mL), extracted with EtOAc (3×50 mL). The combined extracts were washed with brine (20 mL), and dried. Evaporation of the solvent afforded the crude product, which was purified by CombiFlash (eluting with 1–8% MeOH in DCM) to afford (2S,3S)-2-{4'-[(4''-aminophenyl)buta-1',3'-diynyl]benzamido}-1,3-dihydroxy-butanamide (**LPC-053**) (70 mg, 70% yield) as yellow solid. ¹H NMR (300 MHz, DMSO-d₆): δ 1.09 (d, *J*=6.3 Hz, 3H), 3.97 (br s, 1H), 4.23 (t, *J*=16.5 Hz, 1H), 4.94 (br s, 1H), 5.82 (s, 2H), 6.54 (d, *J*=8.4 Hz, 2H), 7.24 (d, *J*=8.7 Hz, 2H), 7.60 (d, *J*=8.1 Hz, 2H), 7.87 (d, *J*=8.7 Hz, 2H), 8.42 (d, *J*=8.7 Hz, 1H), 8.81 (br s, 1H), 10.58 (br s, 1H); ¹³C NMR (75 MHz, DMSO-d₆): δ 21.09, 57.95, 66.84, 71.79, 77.26, 80.83, 86.34, 105.83, 114.27, 124.70, 128.62, 132.55, 134.69, 135.02, 151.54, 165.93, 167.69; HRMS: calculated for C₂₁H₁₉N₃O₄H 378.1454; found 378.1454 [M+H]⁺.

Following the similar procedure, (2R,3R)-2-{4'-[(4''-aminophenyl)buta-1',3'-diynyl]benzamido}-1,3-dihydroxybutanamide (**LPC-054**) and (2R,3S)-2-{4'-[(4''-aminophenyl)buta-1',3'-diynyl]benzamido}-1,3-dihydroxybutanamide (**LPC-055**) were synthesized.

Spectral data for LPC-054—¹H NMR (300 MHz, DMSO-d₆): δ 1.07 (d, *J*=5.4 Hz, 3H), 3.98–4.04 (m, 1H), 4.24 (d, *J*=12.9 Hz, 1H), 4.87 (d, *J*=5.7 Hz, 1H), 5.82 (br s, 2H), 6.53 (d, *J*=8.4 Hz, 2H), 7.24 (d, *J*=8.4 Hz, 2H), 7.63 (d, *J*=8.1 Hz, 2H), 7.90 (d, *J*=6.6 Hz, 2H), 8.13 (d, *J*=7.8 Hz, 1H), 8.84 (br s, 1H), 10.65 (br s, 1H); ¹³C NMR (75 MHz, DMSO-d₆): δ 21.00, 58.80, 67.09, 71.79, 77.29, 80.84, 86.36, 105.84, 114.27, 124.74, 128.59, 132.58, 134.69, 135.02, 151.54, 166.28, 167.62; HRMS: calculated for C₂₁H₁₉N₃O₄H 378.1454; found 378.1453 [M+H]⁺.

Spectral data for LPC-055—¹H NMR (300 MHz, DMSO-d₆): δ 1.09 (d, *J*=6.0 Hz, 3H), 3.95–3.98 (m, 1H), 4.23 (t, *J*=16.2 Hz, 1H), 4.94 (d, *J*=3.9 Hz, 1H), 5.82 (br s, 2H), 6.53 (d, *J*=7.8 Hz, 2H), 7.24 (d, *J*=7.2 Hz, 2H), 7.61 (d, *J*=8.1 Hz, 2H), 7.87 (d, *J*=7.5 Hz, 2H), 8.42 (d, *J*=8.7 Hz, 1H), 8.81 (br s, 1H), 10.58 (br s, 1H); ¹³C NMR (75 MHz, DMSO-d₆): δ 21.09, 57.95, 66.84, 71.79, 77.26, 80.83, 86.34, 105.84, 114.27, 124.70, 128.62, 132.55,

134.69, 135.03, 151.55, 165.93, 167.70; HRMS: calculated for C₂₁H₁₉N₃O₄H 378.1454; found 378.1460 [M+H]⁺.

Construction of *E. coli* W3110PA

P. aeruginosa *lpxC* was used to replace *E. coli* chromosomal *lpxC*. A linear PCR product containing the *P. aeruginosa* *lpxC* with flanking sequences complementary to the upstream 5' region of *E. coli* *lpxC* and to the downstream 3' region of *E. coli* *lpxC*, was amplified from a plasmid carrying *P. aeruginosa* *lpxC* using primers pa-LpxC-5' and pa-LpxC-3' (Table S2). The PCR product was gel purified and electroporated into *E. coli* DY330 cells, which carry λ -red recombinases. While DY330 cannot survive on the LB/agar plate supplemented with 15 μ g/mL of L-161,240, cells wherein *E. coli* *lpxC* replaced with *P. aeruginosa* *lpxC* can survive on this media. Transformants were therefore selected directly using L-161,240. Genomic DNA from resistant colonies was isolated, and the region around *lpxC* was amplified with primers 300-up-*lpxC* and 300-down-*lpxC* and sequenced with primers paLpxC-361-5' and paLpxC-581-3' (Table S2). One clone in which *P. aeruginosa* *lpxC* had replaced chromosomal *E. coli* *lpxC* was selected and grown at 30 °C. This strain was used to generate P1 vir lysate, which was used to transduce chromosomal *P. aeruginosa* *lpxC* into the chromosome of *E. coli* W3110. Transduced cells were plated on LB/agar containing 15 μ g/mL of L-161,240 and 10 mM sodium citrate. The resulting colonies were purified 3 times on this media. Genomic DNA from resistant colonies was isolated, and the region around *lpxC* was amplified with the primers 300-up-*lpxC* and 300-down-*lpxC*, and sequenced with paLpxC-361-5' and paLpxC-581-3'. The colony that harbored the *P. aeruginosa* *lpxC* knock-in was named as W3110PA.

Protein purification, enzyme inhibition and MIC tests

The wild-type *E. coli* LpxC, UDP-3-*O*-[(*R*)-3-hydroxymyristoyl]-*N*-acetylglucosamine, and [α -³²P] UDP-3-*O*-[(*R*)-3-hydroxymyristoyl]-*N*-acetylglucosamine were prepared following established procedures.^{17, 29, 30} Assays of LpxC activity and extraction of K_i^{app} and K_I values were performed as described previously,¹⁸ except that the **LPC-011** concentrations were varied from 0.8 pM to 51 nM. MICs were determined according to the NCCLS protocol adapted to 96-well plates and LB media in the presence of 5% DMSO as described previously.^{18, 31}

X-ray crystallography

Purified *E. coli* LpxC (1–300) samples at a final concentration of 10 mg/mL were mixed with four-fold molar excess of individual compounds. Crystals of *E. coli* LpxC in complex with **LPC-011**, **LPC-012** or **LPC-053** were obtained using the hanging drop vapor diffusion method at 4 °C in solutions containing 0.1 M HEPES pH 7.5, 1.5–1.7 M LiSO₄ and 10 mM DTT. The crystals were cryoprotected with perfluoropolyether (PFO-X175/08) before being flash-frozen in liquid nitrogen. Diffraction data were collected in-house at 100 K using a Rigaku MicroMax-007 HF rotating anode generator and R-Axis IV++ detector. X-ray diffraction data were processed with HKL2000.³² Molecular replacement with PHASER was used to obtain the initial phases of the LpxC-inhibitor complex structures.³³ The structure of the *E. coli* LpxC/**LPC-009** complex (PDB entry 3P3E) was used as the search model. Water molecules were added using PHENIX³⁴ and verified with COOT³⁵. Additional electron density at the protein packing interface is observed in all three *E. coli* LpxC-inhibitor complex crystals. Because this electron density cannot be fitted with the protein or the inhibitor, it likely represents a buffer molecule (e.g., HEPES) or impurity from the chemical synthesis. The final models were obtained after iterative cycles of manual model building with COOT and refinement using PHENIX. MOLPROBITY³⁶ was used to evaluate the quality of the refined structures. The statistics for the LpxC-inhibitor complexes

are shown in Table S1. Structures factors and coordinates for *E. coli* LpxC in complex with **LPC-011**, **LPC-012**, and **LPC-053** have been deposited in the RCSB Protein Data Bank with the accession codes 3PS1, 3PS2, 3PS3, respectively.

Supplementary Material

Refer to Web version on PubMed Central for supplementary material.

Acknowledgments

This research was supported by National Institutes of Health Grants AI055588 (to P.Z.), and GM-51310 (to C.R.H.R). X.L. is supported by the China Scholarship Council. We thank Dr. Nathan I. Nicely for assistance with collection of X-ray diffraction data at the Duke University Crystallography Shared Resource.

References and notes

1. Raetz CRH, Reynolds CM, Trent MS, Bishop RE. *Annu Rev Biochem* 2007;76:295. [PubMed: 17362200]
2. Raetz CRH, Whitfield C. *Annu Rev Biochem* 2002;71:635. [PubMed: 12045108]
3. Barb AW, Zhou P. *Curr Pharm Biotechnol* 2008;9:9. [PubMed: 18289052]
4. Kline T, Andersen NH, Harwood EA, Bowman J, Malanda A, Endsley S, Erwin AL, Doyle M, Fong S, Harris AL, Mendelsohn B, Mdluli K, Raetz CRH, Stover CK, Witte PR, Yabannavar A, Zhu S. *J Med Chem* 2002;45:3112. [PubMed: 12086497]
5. Pirrung MC, Tumey LN, McClerren AL, Raetz CRH. *J Am Chem Soc* 2003;125:1575. [PubMed: 12568618]
6. Anderson, NH.; Bowan, J.; Erwin, A.; Harwood, E.; Kline, T.; Mdluli, K.; Pfister, KB.; Shawar, R.; Wagman, A.; Yabannavar, A. International Patent. WO 2004/062601. 2004.
7. Siddiqui, MA.; Mansoor, UF.; Reddy, PA.; Madison, VS. International Patent. WO 2007/064749. 2007.
8. Moser, H.; Lu, Q.; Patten, PA.; Wang, D.; Kasar, R.; Kaldor, S.; Patterson, BD. International Patent. WO 2008/154642. 2008.
9. Mansoor, UF.; Reddy, P.; Adulla, P.; Siddiqui, MA. International Patent. WO 2008/027466. 2008.
10. Yoshinaga, M.; Ushiki, Y.; Tsuruta, R.; Urabe, H.; Tanikawa, T.; Tanabe, K.; Baba, Y.; Yokotani, M.; Kawaguchi, Y.; Kotsubo, H.; Tsutsui, Y. International Patent. WO 2008/105515. 2008.
11. Mansoor, UF.; Reddy, PA.; Siddiqui, MA. International Paten. WO 2010/017060. 2010.
12. Dobler, MR.; Lenoir, F.; Parker, DT.; Peng, Y.; Piizi, G.; Wattanasin, S. International Patent. WO 2010/031750. 2010.
13. Takashima, H.; Suga, Y.; Urabe, H.; Tsuruta, R.; Kotsubo, H.; Oohori, R.; Kawaguchi, Y. International Patent. WO 2010/024356. 2010.
14. Raju, BG.; O'Dowd, H.; Gao, H.; Patel, DV.; Trias, J. US Patent. 7, 691, 843. 2010.
15. McClerren AL, Endsley S, Bowman JL, Andersen NH, Guan Z, Rudolph J, Raetz CR. *Biochemistry* 2005;44:16574. [PubMed: 16342948]
16. Barb AW, McClerren AL, Snehelatha K, Reynolds CM, Zhou P, Raetz CR. *Biochemistry* 2007;46:3793. [PubMed: 17335290]
17. Barb AW, Jiang L, Raetz CR, Zhou P. *Proc Natl Acad Sci U S A* 2007;104:18433. [PubMed: 18025458]
18. Lee CJ, Liang X, Chen X, Zeng D, Joo SH, Chung HS, Barb AW, Li Y, Toone EJ, Raetz CR, Zhou P. *Chemistry & Biology*. 2010 in press.
19. Glaser C. *Berichte der deutschen chemischen Gesellschaft* 1869;2:422.
20. Nicolaou KC, Zipkin RE, Petasis NA. *J Am Chem Soc* 1982;104:5558.
21. Sonogashira K, Tohda Y, Hagihara N. *Tetrahedron Lett* 1975;16:4467.
22. Elliott DF. *J Chem Soc* 1950:62.
23. Andersson PG, Guijarro D, Tanner D. *J Org Chem* 1997;62:7364. [PubMed: 11671853]

24. Meldal M, Tornøe CW. *Chem Rev* 2008;108:2952. [PubMed: 18698735]
25. Gennadios HA, Christianson DW. *Biochemistry* 2006;45:15216. [PubMed: 17176043]
26. Buetow L, Dawson A, Hunter WN. *Acta Crystallograph Sect F Struct Biol Cryst Commun* 2006;62:1082.
27. Barb AW, Leavy TM, Robins LI, Guan Z, Six DA, Zhou P, Hangauer MJ, Bertozzi CR, Raetz CR. *Biochemistry* 2009;48:3068. [PubMed: 19256534]
28. Jencks WP. *Proc Natl Acad Sci U S A* 1981;78:4046. [PubMed: 16593049]
29. Mochalkin I, Knafels JD, Lightle S. *Protein Sci* 2008;17:450. [PubMed: 18287278]
30. Jackman JE, Raetz CRH, Fierke CA. *Biochemistry* 2001;40:514. [PubMed: 11148046]
31. Wikler, MA.; Low, DE.; Cockerill, FR.; Sheehan, DJ.; Craig, WA.; Tenover, FC.; Dudley, MN. Clinical and Laboratory Standards Institute (Formally NCCLS). 2006.
32. Otwinowski Z, Minor W. *Methods Enzymol* 1997;276:301.
33. McCoy AJ, Grosse-Kunstleve RW, Adams PD, Winn MD, Storoni LC, Read RJ. *J Appl Crystallogr* 2007;40:658. [PubMed: 19461840]
34. Zwart PH, Afonine PV, Grosse-Kunstleve RW, Hung LW, Ioerger TR, McCoy AJ, McKee E, Moriarty NW, Read RJ, Sacchettini JC, Sauter NK, Storoni LC, Terwilliger TC, Adams PD. *Methods Mol Biol* 2008;426:419. [PubMed: 18542881]
35. Emsley P, Cowtan K. *Acta Crystallogr D Biol Crystallogr* 2004;60. [PubMed: 15608376]
36. Davis IW, Leaver-Fay A, Chen VB, Block JN, Kapral GJ, Wang X, Murray LW, Arendall WB 3rd, Snoeyink J, Richardson JS, Richardson DC. *Nucleic Acids Res* 2007;35. [PubMed: 17148476]

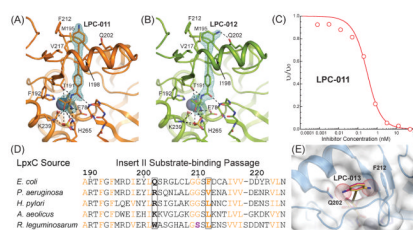


Figure 1.

Structural and biochemical characterization of **LPC-009** derivatives with amino substitutions at the distal phenyl ring. (A) Structure of the *E. coli* LpxC/**LPC-011** complex. (B) Structure of the *E. coli* LpxC/**LPC-012** complex. LpxC is shown in the ribbon diagram. Inhibitors, LpxC residues important for inhibitor binding, and a sulfate molecule in the active site are shown in the stick model. Blue meshes represent the Fo-Fc omit map (contoured at 3.4σ) surrounding the inhibitors. The active site zinc ion is shown in a space-filling model. Hydrogen bonds are denoted as dashed lines. (C) Inhibition curve of **LPC-011** against *E. coli* LpxC. (D) Sequence alignment of the Insert II substrate-binding passage. Conserved hydrophobic residues and the two Gly residues at the exit of the substrate binding passage (G209 and G210 in *E. coli* LpxC) are colored in orange. S214 in *R. leguminosarum* LpxC (corresponding to G210 in *E. coli* LpxC), which is the main cause of **CHIR-090** resistance, is colored in purple. Residues predicted to clash with **LPC-013** are boxed. Sequence alignment includes LpxC orthologs from *Escherichia coli*, *Pseudomonas aeruginosa*, *Helicobacter pylori*, *Aquifex aeolicus*, and *Rhizobium leguminosarum*. (E) Docking model of **LPC-013** bound to *E. coli* LpxC based on the **LPC-011** complex structure, illustrating vdW clashes between the *ortho*-amino group with residues in the Insert II substrate-binding passage.

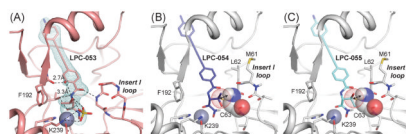
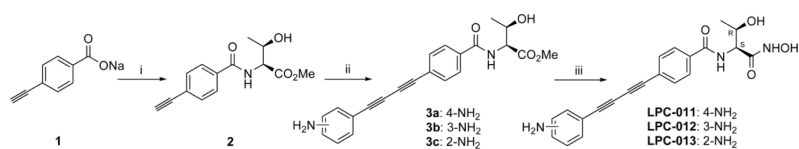
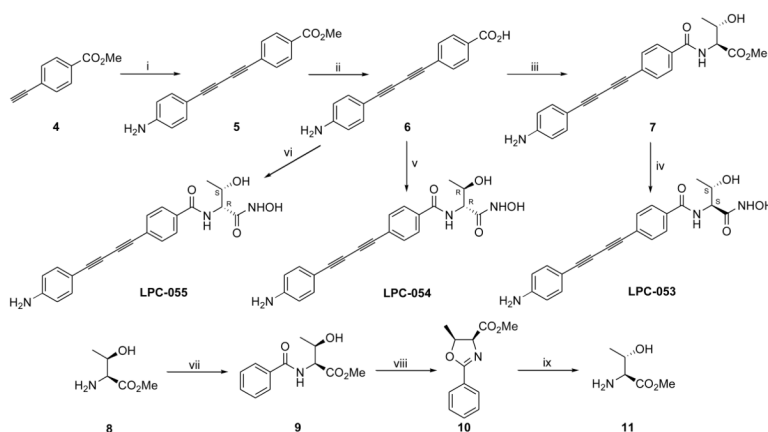


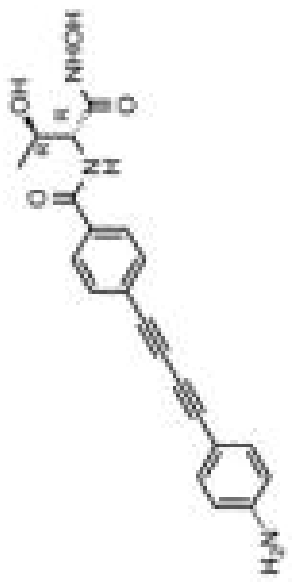
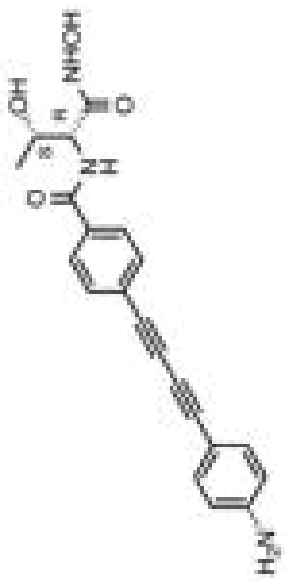
Figure 2. Stereochemical requirement of the threonyl group of LpxC inhibitors in the active site. (A) Structure of **LPC-053** bound to *E. coli* LpxC. LpxC is shown in the ribbon diagram. Blue meshes represent the Fo-Fc omit map (contoured at 3.4σ) surrounding the inhibitor. The active site zinc ion is shown in a space-filling model. **LPC-053**, LpxC residues important for inhibitor binding, and a sulfate molecule in the active site are shown in the stick model. Hydrogen bonds are denoted as dashed lines. Structural models of **LPC-054** and **LPC-055** complexes (based on the structures of **LPC-011** and **LPC-053** complexes) are shown in (B) and (C), respectively, illustrating vdW clashes between the side-chain of the inhibitor threonyl group and backbone residues in the Insert I loop of LpxC.

**Scheme 1.**

Reagents and conditions: (i) L-threonine methyl ester hydrochloride, EDC.HCl, HOBt, DIEA, DMF, 0 °C, 1 h, then room temperature, 20 h, 48%. (ii) substituted acetylene, Cu(OAc)₂, pyridine, MeOH, room temperature. (iii) H₂NOH.HCl, 25% NaOMe/MeOH, THF, 0 °C, 2 h, then room temperature, 16 h.

**Scheme 2.**

Reagents and conditions: (i) 4-ethynylbenzamide, $\text{Cu}(\text{OAc})_2$, pyridine, MeOH, room temperature, 48 h, 35%. (ii) 3 N NaOH, MeOH, reflux, 1 h, 90%. (iii) **11**, EDC.HCl, HOBT, DIEA, DMF, 0 °C, 1 h, then room temperature, 18 h, 92%. (iv) $\text{H}_2\text{NOH.HCl}$, 25% NaOMe/MeOH, THF, 0 °C, 2 h, then room temperature, 14 h, 70%. (v) (1) D-threonine, SOCl_2 , MeOH, reflux, 1 h, 99%; (2) **6**, EDC.HCl, HOBT, DIEA, DMF, 0 °C, 1 h, then room temperature, 18 h, 92%. (3) $\text{H}_2\text{NOH.HCl}$, 25% NaOMe/MeOH, THF, 0 °C, 2 h, then room temperature, 14 h, 93%. (vi) (1) *allo-D*-threonine, SOCl_2 , MeOH, reflux, 1 h, 99%; (2) **6**, EDC.HCl, HOBT, DIEA, DMF, 0 °C, 1 h, then room temperature, 18 h, 69%. (3) $\text{H}_2\text{NOH.HCl}$, 25% NaOMe/MeOH, THF, 0 °C, 2 h, then room temperature, 14 h, 69%. (vii) benzoyl chloride, Et_3N , MeOH, 0 °C, 2 h, 92%. (viii) SOCl_2 , 0 °C, 5 days, 94%. (ix) (1) 6 N HCl, reflux, 5 h; (2) SOCl_2 , MeOH, reflux, 1 h, 98%.

| Name | Structure | MIC (µg/mL) | | | |
|---------|------------------------------------------------------------------------------------|--------------------------|------------------------|------------------------|---------------------------|
| | | <i>E. coli</i> Wild type | <i>E. coli</i> W3110RL | <i>E. coli</i> W3110PA | <i>P. aeruginosa</i> PAOI |
| LPC-054 |  | 6.3 | >25 | >25 | >25 |
| LPC-055 |  | 3.1 | >25 | >25 | >25 |